ARMA 23-721

Shearing and opening of a pre-existing discontinuity in response to fluid injection

Lecampion, B., Sáez A. and Gupta, A.

Geo-Energy Lab - Gaznat chair, Ecole Polytechnique Fédérale de Lausanne (EPFL), Lausanne, Vaud, Switzerland

ABSTRACT: We investigate the fluid-driven growth of a shear crack along a frictional discontinuity and its transition to hydraulic fracturing (sometimes referred to as hydraulic jacking) under plane-strain conditions. We focus on the case of a constant friction coefficient and account for the permeability changes associated with the fracture opening. By combining the scaling analysis and numerical simulations, we examine the evolution of both the shear and opening fronts as a function of the hydro-mechanical properties of the pre-existing discontinuity, in-situ stress state, and the fluid injection conditions. Further, we derive an approximate analytical solution for the relation between the positions of the slip and opening fronts at large times. We notably show that the ratio between the slip and opening fronts converges to a constant value at late times which only depends on the ratio between the shear stress and shear strength acting initially along the discontinuity. We compare this approximate solution against numerical simulations and demonstrate its usage to serve as a benchmark solution in the development of coupled hydro-mechanical numerical solvers for frictional fluid-driven fractures.

1 INTRODUCTION

Hydraulic stimulation of pre-existing fractures is used in the geothermal development in order to increase reservoir permeability and achieve economical flow rates - with mixed success (Jung, 2013; McClure and Horne, 2014). Although the primary idea is to shear dilate these pre-existing discontinuities via injection, in a number of field tests (Guglielmi et al., 2020), a large increase of permeability is only observed when fracture opening has been reached (sometimes denoted as hydraulic jacking). Shearing of pre-existing discontinuities can also occur during more traditional hydraulic fracturing operations in oil and gas reservoirs, either by direct fluid pressurization or via stress transfer from the main fractures. In this contribution, we investigate the fluid-driven growth of a shear crack along a frictional discontinuity and its transition to hydraulic fracturing. We focus on the case of a constant friction coefficient and account for permeability changes associated with fracture opening. We use a fully coupled implicit numerical scheme for the solution of this non-linear hydro-mechanical problem. Notably, the frictional interface behavior is modeled using an elastoplastic constitutive relation with a non-associated flow rule.

Building on previous works (Hayashi and Abe, 1982; Detournay, 2016; Azad et al., 2017), we combine a scaling analysis with numerical simulations to investigate the evolution of the shear and opening fronts in terms of the properties of the pre-existing discontinuities (friction and initial hydraulic properties), the in-situ and injection conditions.

2 PROBLEM FORMULATION

This study aims to understand the effect of the injection of a Newtonian fluid under a constant rate on the activation and propagation of a shear rupture, which as the fluid pressurization continues lead to the initiation and propagation of an opening mode fluid driven rupture. In other words, how fluid injection under a constant rate in a pre-existing fracture transition from shearing to opening mode hydraulic fracturing (sometimes also denoted hydraulic jacking in the geothermal community). We restrict our discussion to a two-dimensional plane-strain configuration as sketched in Fig.1.

2.1. Solid mechanics

We consider the case of a pre-existing planar discontinuity (fracture/fault) embedded in an isotropic homogeneous

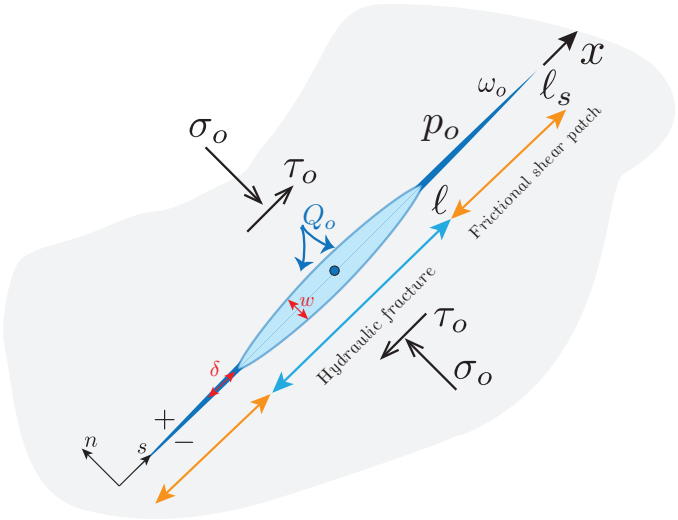

Fig. 1: Sketch of the injection into a pre-existing fracture of initial aperture ω_o. Upon injection at a constant rate, a frictional shear rupture is first propagated, then a zero-toughness hydraulic fracture. ℓ_s and ℓ denote the position of the tip of the frictional rupture and the opening patch, respectively.

linearly elastic medium under uniform background stress and pore-pressure fields. The elastostatic balance of momentum can be written as the following boundary integral equation relating the traction T_i and the displacement discontinuity $d_i = u_i^+ - u_i^-$ vectors on the pre-existing fracture:

$$T_i(x,t) - T_i^o(x,t) = -\int_{\Gamma_f} \mathbb{H}_{ij}(x,y) \cdot d_j(y,t)\, \mathrm{d}S_y \qquad (1)$$

where $i,j = s,n$ with s and n the tangential and normal components along the fracture, $\mathbb{H}_{ij}$ is the elastostatics hyper-singular kernel (Hills et al., 1996; Mogilevskaya, 2014) which embeds the elastic properties of the medium, and T_i^o denotes the initial in-situ tractions (prior to any deformation). The elastostatics hyper-singular kernel depends on the elastic material properties of the surrounding rock of the preexisting discontinuity, namely Young's modulus E and shear modulus μ. It is important to recall that for the case of a planar discontinuity Γ_f, the hyper-singular kernel uncouples (i.e., $\mathbb{H}_{sn} = \mathbb{H}_{ns} = 0$) such that fracture slip does not induce any change in normal traction and similarly fracture opening does not induce any shear traction. In the local frame of reference of the pre-existing discontinuity, we denote the fracture slip $d_s = \delta$, the fracture opening $d_n = w$, and the shear and normal tractions $T_s = \tau$ and $T_n = \sigma$ respectively.

We introduce the effective traction vector T_i' acting on the interface Γ_f by subtracting the effect of pore-pressure p on the normal traction: $T_i' = T_i - p\delta_{in}$ (where δ_{ij} the Kronecker delta). We assume a Mohr-Coulomb criterion without cohesion for the yielding of this interface. We consider a constant friction coefficient f, such that in the convention of positive stress in compression, the yield criterion reads:

$$F(T_i') = |\tau| - f \cdot (\sigma - p) \leq 0 \qquad (2)$$

Accounting for the presence of a gouge material and/or asperities within the interface, we write a local elasto-plastic constitutive relation for the interface following traditional modeling approaches of rock joints (see Plesha (1995); Mroz and Giambanco (1996); Stupkiewicz and Mróz (2001) among others). We split the rate of displacement discontinuity $\dot{d}_i$ in an elastic and plastic part $\dot{d}_i = \dot{d}_i^e + \dot{d}_i^p$, and introduce an elastic spring-like stiffness of the contact relating effective tractions and the elastic part of the displacement discontinuity:

$$\dot{T}_i' = C_{ij} \cdot (\dot{d}_j - \dot{d}_j^p) \qquad (3)$$

$$C_{ij} = K_s s_i \otimes s_j + K_n n_i \otimes n_j \qquad (4)$$

where implicitly, we assume the interface filling material/asperities to behave as a "granular" material (such that the poroelastic Biot coefficient is unity). We restrict hereafter to the case of constant stiffness in the shear K_s and normal K_n directions. The case of a rigid plastic interface is obtained numerically in the limit of large interface stiffness in comparison to the bulk rock material.

Interface plastic displacement discontinuity is activated when the yield function is reached ($F = 0$), and we assume non-associated Mohr-Coulomb plastic flow with a constant dilatant coefficient $\psi < f$:

$$\dot{d}_i^p = \dot{\lambda} \frac{\partial G}{\partial T_i'}, \qquad \dot{\lambda} > 0 \text{ when } F(T_i') = 0, \qquad (5)$$

and $\dot{\lambda} = 0$ when yield is not activated ($F(T_i') < 0$). We use a simple non-associated plastic potential $G = |\tau| - \psi \cdot (\sigma - p)$, and restrict in the remainder of this paper to the non-dilatant case $\psi = 0$ which corresponds to the limit of a "mature" interface over which sufficient irreversible deformation have to occur such that it can be considered to be at "critical state" within the terminology of geomaterials.

2.2. *Fluid flow*

We restrict to the case of an impermeable rock matrix such that the fluid flow occurs solely inside the pre-existing discontinuity. Denoting as $m_f = \rho_f \phi$ the fluid mass per unit volume of the material filling the interface, where ϕ is the interface porosity and ρ_f the fluid density, the total fluid mass integrated over the thickness ω of the interface is simply ωm_f. We write the thickness of the interface as $\omega = \omega_o + w$ (with ω_o its initial thickness), such that for a liquid-filled interface, the width-averaged balance of fluid

mass for a two-dimensional plane-strain configuration can be re-expressed as the following fluid volume balance:

$$\frac{\partial w}{\partial t} + \omega S \frac{\partial p}{\partial t} + \frac{\partial \omega v}{\partial x} = \delta(x) Q_o \tag{6}$$

The injection is carried at a constant 2D rate Q_o directly in the interface (see Fig.1). S denotes the storage coefficient of the interface, which combines the liquid and interface-filling material pore compressibilities. The width-averaged fluid velocity v is given by Darcy's law

$$v = -\frac{k(w)}{\mu} \frac{\partial (p - p_o)}{\partial x} \tag{7}$$

where μ is the fluid viscosity, and p_o the initial pore-pressure. The interface intrinsic permeability k is highly dependent on the variation of the aperture. In the limit of an open fracture, k is given by Poiseuille's law such that $k = w^2/12$. It is well known that for low mechanical aperture ($w \ll \omega_o$), the 'cubic law' $\omega k = w^3/12$ underestimates the flow transmissibility which tends to a constant value (Witherspoon, P. A. and Wang, J. S.Y. and Iwai, K. and Gale, J. E., 1980). In order to bridge from the mechanically closed to the mechanically open state, we write the permeability - fracture opening relation as:

$$k(w) = (\omega_o^h + w)^2/12 \tag{8}$$

where ω_o^h is an equivalent hydraulic aperture at small mechanical aperture ($w \ll \omega_o$). ω_o^h can be expressed as $\sqrt{12 k_o}$ where k_o is the initial interface permeability. In this study, we assume $\omega_o = \omega_o^h$ which corresponds to the case of a pre-existing fracture with no filling material.

3 LIMITING REGIMES

Prior to the hydraulic opening of the interface, in the absence of shear-induced dilatancy ($\psi = 0$) and very high elastic modulus of the interface ($K_n \gg E/\omega$), the fault has a constant permeability k_o. In that limit, the shear rupture of the interface does not influence the interface hydraulic properties. The knowledge of the pore-pressure evolution along the fracture allows solving for the evolution of the corresponding frictional shear crack. A number of solutions have been recently obtained for fluid-induced shear ruptures (Bhattacharya and Viesca, 2019; Viesca, 2021; Sáez et al., 2022).

On the other hand, in the limit where the fracture is oriented such that it does not hold any initial shear stress (τ_o), the fluid injection will solely result in the triggering of a tensile rupture. If the initial interface permeability is negligible, the configuration is strictly one of the propagation of a hydraulic fracture in an impermeable medium with zero fracture toughness. Solutions for the evolution of such hydraulic fracture in the plane-strain configuration are known Adachi and Detournay (2002); Garagash and Detournay (2005).

We discuss these limiting cases below in more detail and formulate scaling arguments for the case of a hydraulic fracture with a frictional shear-activated patch ahead of its tips (see Fig. 1).

Suppose we restrict to the case of a rigid plastic interface (infinite interface stiffness). In that case, the elastic boundary integral equations can be written solely on the parts of the interface for which the Mohr-Coulomb yield condition is active. In the configuration investigated here, where the rupture propagation is driven by a point injection, the rupture will evolve symmetrically from the injection point (Fig.1). We denote $\ell_s(t)$ the position of the frictional shear rupture tip (for which the yielding condition is first reached), and $\ell(t)$ the position at which the effective normal traction reaches zero for the first time (such that the fracture opens). Further, $\ell_s(t) \geq \ell(t)$ owing to the fact that frictional failure occurs prior to the moment when the normal effective traction $\sigma - p$ becomes zero. Note that in the opening zone, for $x \leq \ell(t)$, σ equals the fluid pressure p and the shear traction τ vanishes.

3.1. *Frictional shear rupture driven by injection at constant rate*

Let's first recall the case where interface opening is not reached: in other words, when the fluid pressure at the injection point always remains below the in-situ normal traction σ_o. The solution for the activation and propagation of a frictional rupture (with a constant friction coefficient) has been recently derived (see appendix D of Sáez et al. (2022)). Under the assumption of constant thickness ($w = 0$) and constant hydraulic properties in Eqs (6)-(7), the pore-pressure evolution along the interface is given by the solution of the diffusion equation:

$$S \frac{\partial p}{\partial t} - \frac{k_o}{\mu} \frac{\partial^2 p}{\partial x^2} = \delta(x)(Q_o/w_o) \tag{9}$$

which is given by Carslaw and Jaeger (1959):

$$\begin{aligned} p(x,t) &= p_o + \frac{Q_o \mu}{2\sqrt{\pi} k_o \omega_o} \sqrt{4\alpha t}\, \Pi_f(\xi) \\ \Pi_f(\xi) &= \exp(-\xi^2) - \sqrt{\pi}|\xi| \mathrm{Erfc}(|\xi|) \\ &\text{with } \xi = \frac{x}{\sqrt{4\alpha t}} \end{aligned} \tag{10}$$

where $\alpha = k_o/(\mu S)$ is the hydraulic diffusivity, and $\Pi_f(0) = 1$. The location of the nominal pore-pressure diffusion front evolves as the square root of time $\ell_d = \sqrt{4\alpha t}$. Due to the increase of pore pressure, the shear crack is

activated in shear when $fp = f\sigma_o - \tau_o$. Denoting $\sigma'_o = \sigma_o - p_o$, the time at which the frictional rupture initiates (using $\xi = 0, t = t_s, p = \sigma_o - \tau_o/f$, in Eq. (10)) is simply

$$t_s = \left(\frac{\sqrt{\pi} k_o \omega_o (f\sigma'_o - \tau_o)}{f Q_o \mu \sqrt{\alpha}} \right)^2, \tag{11}$$

and the corresponding position of the pore-pressure diffusion front provides the corresponding characteristic length scale

$$L_s = \sqrt{4\alpha t_s} = \frac{\sqrt{4\pi} k_o \omega_o (f\sigma'_o - \tau_o)}{f Q_o \mu} \tag{12}$$

The evolution of the shear crack with time is obtained by recognizing that the stress should not be singular at the tip of the rupture of such a frictional crack, and therefore the mode II stress intensity factor must be zero (Garagash and Germanovich, 2012; Bhattacharya and Viesca, 2019; Viesca, 2021). For the case of constant injection rate, Sáez et al. (2022) shows that at late times ($t \gg t_s$), the rupture evolves linearly with the time t, such that $\ell_s = (L_s/\sqrt{4\pi}) \times t/t_s$.

3.2. Initiation of hydraulic fracturing

As previously mentioned, the shear slip does not modify the normal stress along the plane of discontinuity, we can thus readily obtain the expression for the onset of the hydraulic opening using the evolution of the pore pressure (Eq. (10)). Therefore, the time t_o at which the pore pressure at the injection point reaches the in-situ normal stress σ_o corresponds to the onset of the opening rupture, and (using $\xi = 0, t = t_o, p = \sigma_o$, in Eq. (10)) is given by:

$$t_o = t_s/(1 - \mathcal{S})^2, \tag{13}$$

where $\mathcal{S} = \tau_o/(f\sigma'_o)$ is the initial stress criticality. The corresponding pore-pressure diffusion length scale is given by

$$L_o = \sqrt{4\alpha t_o} = L_s/(1 - \mathcal{S}). \tag{14}$$

3.3. Zero toughness hydraulic fracture

In the absence of initial shear stress τ_o, only a tensile opening hydraulic fracture initiates. In the limit of negligible initial interface permeability ($\omega_o \to 0$), the configuration corresponds to the case of a hydraulic fracture propagating in a medium with zero fracture toughness: the presence of the interface implies that no energy is spent in creating new surfaces. The plane-strain hydraulic fracture propagation solution for the case of a Newtonian fluid is known (Adachi and Detournay, 2002; Garagash and Detournay, 2005; Detournay, 2004) and reads:

$$\ell(t) = \gamma_m L_m(t) \tag{15}$$

$$w(x,t) = \epsilon_m(t) L_m(t) \Omega_m(\xi = x/\ell) \tag{16}$$

$$\sigma(x) - \sigma_o = \Delta\sigma(x) = \epsilon_m(t) E' \Pi_m(\xi = x/\ell) \tag{17}$$

with the self-similar characteristic hydraulic fracture length L_m and aspect ratio ϵ_m given by

$$L_m(t) = \frac{E'^{1/6} Q_o^{1/2} t^{2/3}}{(12\mu)^{1/6}} \qquad \epsilon_m(t) = \frac{(12\mu)^{1/3}}{E'^{1/3} t^{1/3}} \tag{18}$$

The dimensionless solution $(\gamma_m, \Omega_m, \Pi_m)$ can be found in Adachi and Detournay (2002); Detournay (2004). The complete expression for the stress perturbation ahead of the fracture tip has been obtained in Azad et al. (2017). These expressions are not repeated here. Note that the shear stress induced by an opening mode fracture is zero along the fracture plane (uncoupling of the elastostatic boundary integral equations for a single planar interface).

The hydraulic fracture influences the normal stress ahead of the fracture (unclamping). In the presence of a non-zero initial shear stress, for which a frictional patch exists ahead of the fracture, the hydraulic fracture "drives" the behavior of the frictional patch via the normal effective stress variation ahead of its tip. In the limit of an "impermeable" interface initially, the normal effective stress $\sigma' = \sigma - p$ reduces to

$$\sigma' = \sigma'_o + (1 - B')\Delta\sigma(x) \tag{19}$$

where $B' = \dfrac{2}{3} B(1 + \nu_u)$ is the plane-strain Skempton coefficient of the interface filling material (Rice and Cleary, 1976) which relates the undrained pore-pressure response Δp_u and the change in normal stress induced by the hydraulic fracture $\Delta\sigma(x)$. Note that we can similarly relate the undrained pore-pressure response - from Eqs. (4)) and (6) - to the storage coefficient and the normal interface stiffness

$$\Delta p_u = \Delta\sigma'/(\omega K_n S) - \Delta w^p/(\omega S) \tag{20}$$

In this study, we restrict to the case of a 'stiff' interface ($K_n \to \infty$), and zero plastic dilatancy associated with slip (Δw^p=0). As a result, the undrained pore-pressure response ahead of the crack is thus strictly zero $\Delta p_u = 0$ (which corresponds to the case $B' = 0$).

3.4. Large time solution for the shear crack patch ahead of the opening tip

Azad et al. (2017) have investigated the problem of hydraulic fracturing of a pre-existing fault having a given initial shear stress τ_o and the possible nucleation of a dynamic rupture ahead of the opening tip, using a slip weakening friction coefficient. We briefly recall their approach for the relevant case of a constant friction coefficient below.

At the large time ($t \gg t_o$ and thus $t \gg t_s$), the hydraulic fracture governs the shear-slip patch via the change of effective normal stress. For a constant friction coefficient,

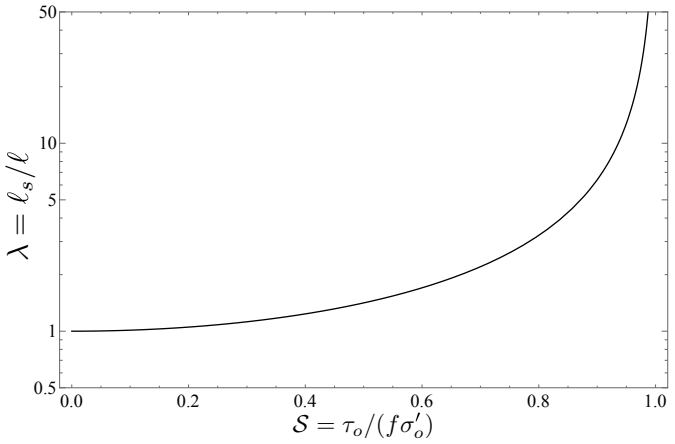

Fig. 2: Large time solution for the ratio of the frictional shear patch tip position over the hydraulic fracture front tip position $\lambda = \ell_s/\ell$ as a function of the stress criticality $\mathcal{S}$ of the pre-existing fracture.

the mode II stress intensity factor at the tip of the frictional crack must be zero. Using the plane-strain expression of the stress intensity factor, this condition reads (Rice, 1968; B.A. Bilby and J.D. Eshelby, 1968)

$$0 = \int_{-\ell_s}^{\ell_s} \frac{\tau(x,t) - \tau_o}{\sqrt{\ell_s^2 - x^2}} \, \mathrm{d}x \tag{21}$$

The shear stress inside the frictional rupture satisfies the Mohr-Coulomb criterion, notably, we have

$$\tau(x,t) = \begin{cases} 0 & \text{for } |x| \in [0, \ell(t)] \\ f \cdot (\sigma'_o + (1-B')\Delta\sigma(x)) & \text{for } |x| \in [\ell(t), \ell_s(t)] \end{cases} \tag{22}$$

Introducing the zero-toughness (viscosity-dominated) solution in Eqns. (21)-(22) and the change of variable $\xi = x/\ell$ yields an implicit equation for $\lambda(t) = \ell_s/\ell$:

$$\int_{-1}^{1} \frac{-\mathcal{S}}{\sqrt{\lambda^2 - \xi^2}} \, \mathrm{d}\xi + 2\int_{1}^{\lambda} \frac{(1-\mathcal{S}) + \mathcal{P}(t)\Pi_m(\xi)}{\sqrt{\lambda^2 - \xi^2}} \, \mathrm{d}\xi = 0 \tag{23}$$

with $\mathcal{S} = \tau_o/(f\sigma'_o)$ is the initial stress criticality and

$$\mathcal{P}(t) = \frac{f(1-B')E'\epsilon_m(t)}{f\sigma'_o} = \frac{(1-B')E'^{2/3}(12\mu)^{1/3}}{\sigma'_o t^{1/3}} \tag{24}$$

We thus identify another time-scale t_p related to the time at which the normal stress perturbation due to the opening patch is of order one, i.e., when $\mathcal{P}(t_p) = 1$:

$$t_p = \frac{(1-B')^3 E'^2 (12\mu)}{\sigma'^3_o} \tag{25}$$

For times much larger than t_p ($\mathcal{P} \ll 1$), the size of the dimensionless frictional patch $\lambda = \ell_s/\ell$ ahead of the opening front will tend to be a constant solely function of stress criticality $\mathcal{S}$. In the limit $\mathcal{P} = 0$, Eq. (23) gives the following implicit equation for λ as a function of $\mathcal{S}$, $\mathrm{arccosec}(\lambda)/\mathrm{arcsec}(\lambda) = (1-\mathcal{S})/\mathcal{S}$. The results of this large-time limit are reported in Fig. 2.

4 NUMERICAL SIMULATIONS

We now test the transitions toward the previously discussed limiting solutions via fully-coupled simulations.

4.1. Description of the solver

We are currently developing a fully-coupled solver for the solution of fluid-driven ruptures to allow the simulation of fluid injection into multiple pre-existing fractures (see (Sáez et al., 2022; Ciardo and Lecampion, 2023; Ciardo et al., 2020; Ciardo and Lecampion, 2019) for some previously reported work in that direction). We briefly outline here the main ingredients of this algorithm. The quasi-static linearly elastic equilibrium (Eq. (1)) is solved via a boundary element method using piece-wise continuous shape functions for the displacement jumps across the fractures. We accelerate the boundary element method using an in-house multi-threaded implementation of hierarchical matrix algorithms (Hackbusch, 2015). In particular, our algorithm is specifically tailored for vectorial boundary integral equations (Ciardo et al., 2020). The pre-existing interface is meshed with a fixed number of elements. The elastoplastic interface constitutive relations allow us to solve for the displacement jumps as the primary unknowns. A fully implicit backward Euler time integration scheme is used to solve in a fully-coupled manner for the mechanical equilibrium (1), the non-linear interface mechanical behavior (4-5), and the fluid flow along the interfaces (6-7) Fluid flow in the fracture is discretized spatially with finite elements. The resulting non-linear system for the increment of fluid pressures and displacement discontinuities over a time step is solved using a Newton-Raphson algorithm. The elastoplastic behavior of the interface is solved via a classical elastic predictor/plastic corrector scheme. We notably use the consistent tangent operator relating the local increment of effective tractions to the total displacement discontinuity vector- thus ensuring quadratic convergence of the Newton-Raphson procedure. At each iteration of the Newton scheme, the coupled hydro-mechanical Jacobian system is solved by a GMRES iterative algorithm using a specific block-upper preconditioner. Finally, the time-step is automatically adapted using an approximation of the local truncation error similar to the one discussed in Sheng and Sloan (2003).

4.2. Strictly tensile hydraulic re-opening

In order to verify this numerical scheme, we first benchmark it against the zero-toughness hydraulic fracture solu-

Table 1: Set of parameters used in the reported simulations.

	Set 1	Set 2
τ_o (MPa)	0	6
σ'_o (MPa)	15	15
p_o (MPa)	0	0
E' (GPa)	41.66	41.66
K_n	100 E'	100 E'
K_s	100 E'	100 E'
f (-)	0.6	0.6
S (Pa^{-1})	$1.\cdot10^{-10}$	$1.\cdot10^{-10}$
$\omega_o = \omega_o^h$ (m)	$5\cdot10^{-6}$	$5\cdot10^{-6}$
12μ (Pa·s)	1.0	1.0
α (m^2·s^{-1})	1.0	1.0
Q_o (m^2·s^{-1})	$5\cdot10^{-6}$	$5\cdot10^{-6}$
$\mathcal{S}$	0	0.4
t_s (s)	$6.3\cdot10^{-5}$	$1.017\cdot10^{-5}$
L_s (m)	0.015	0.00638
t_o/t_s	1	2.777
L_o/L_s	1	1.666
t_p (s)	0.51	0.51
$\lambda(t \gg t_p)$	1	1.236

tion in plane-strain conditions (see Sec. 3.3). The material properties used for this simulation are listed in Table 1 (set 1). It is important to note that in this numerical simulation, the interface has a small but finite initial permeability and large but finite elastic stiffness. As a result, the tip of the opening mode hydraulic fracture is "leaky" as we don't explicitly impose the zero fluid flux boundary condition ahead of the hydraulic fracture tip. This condition is not warranted in the case of pre-existing interface with finite permeability discussed in this work.

Fig. 3 displays the time evolution of the "open" part of the interface (half of it owing to the problem symmetry). The corresponding relative error to the zero-toughness hydraulic fracture growth solution is reported in Fig. 4. We observe a very good convergence toward the analytical solution as the number of elements within the open patch increases. Notably, the relative error decreases as $t^{-2/3}$, which hints that the absolute difference between the numerical solution and the hydraulic fracture solution tends to a constant (most likely related to the "leaky" tip and finite discretization in the numerical solution). Note that this simulation was performed with a uniform mesh of 2000 elements of 0.01 meter size. The impact of the "leaky" tip can be clearly observed in Fig. 5 where the fluid pressure profile at a given time is reported for both the numerical solution and the zero toughness hydraulic fracture solution. The latter has a negative pressure singularity at the tip, which is 'regularized' in the numerical solution in association with the initial permeability of the interface. A pressure drop below the initial fluid pressure

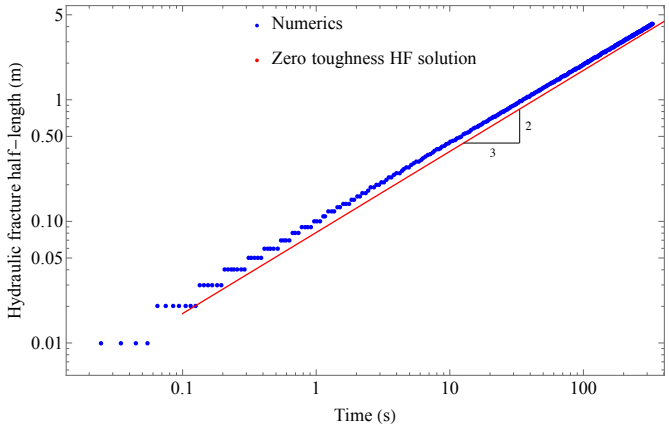

Fig. 3: Evolution of the half-length of the opening rupture - numerical versus the zero-toughness hydraulic fracture solution of Adachi and Detournay (2002) (Parameters set # 1 of Table‘1).

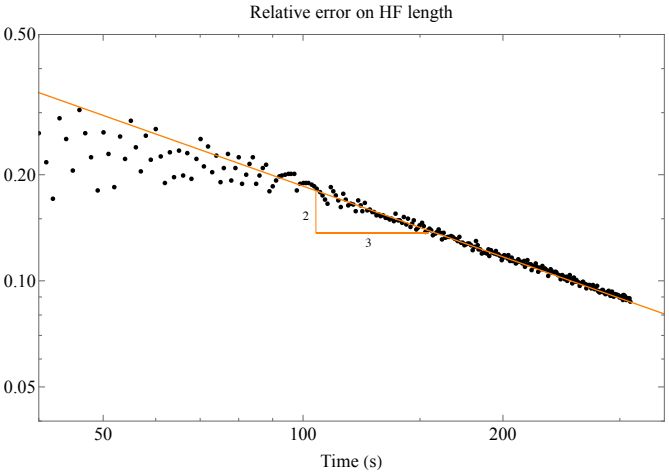

Fig. 4: Time-evolution of the relative error between the numerical estimation of half-length of the opening rupture with respect to the zero-toughness hydraulic fracture solution of Adachi and Detournay (2002).

can be observed at the opening front.

4.3. Shearing and opening of a frictional interface

We now investigate the case of a non-zero initial shear stress on the pre-existing fracture, keeping all the other parameters the same (set # 2 in Table 1, as well as mesh-size).

Fig. 6 displays the evolution of both the tip of the frictional rupture ℓ_s and the hydraulic fracture tip ℓ with time. The corresponding ratio $\lambda = \ell_s/\ell$ can be visualized on Fig. 7. We can observe that although λ tends to be a constant, its convergence toward the late-time solution $\lambda(\mathcal{S} = 0.4) = 1.236$ is not yet achieved at the end of this simulation. This can be partly explained by the fact that the opening tip location remains further away from the zero-toughness hydraulic fracture solution for the same in-

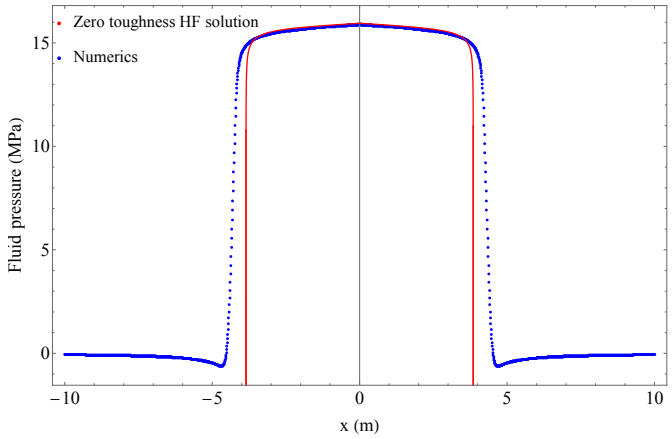

Fig. 5: Fluid pressure profiles (at $t = 328s$) - zero initial shear-stress case (Parameters set # 1 of Table 1).

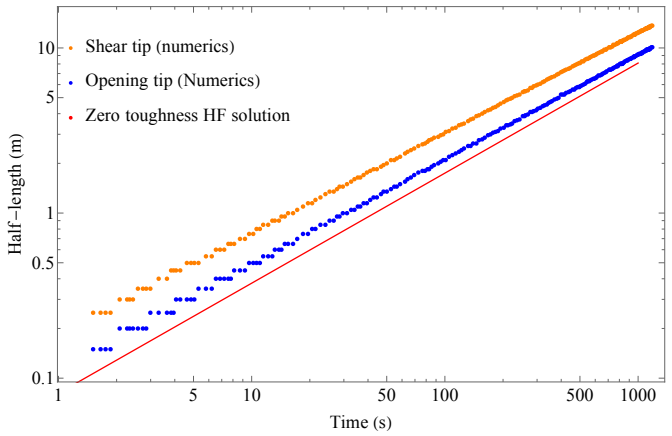

Fig. 6: Evolution of the shear and opening front position with time - $\mathcal{S} = 0.4$ case (Parameters set # 2 of Table 1).

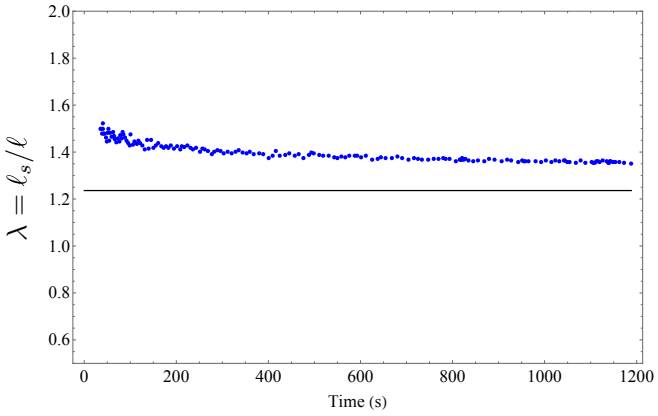

Fig. 7: Evolution of the shear to opening front position with time - $\mathcal{S} = 0.4$ case (Parameters set # 2 of Table 1).

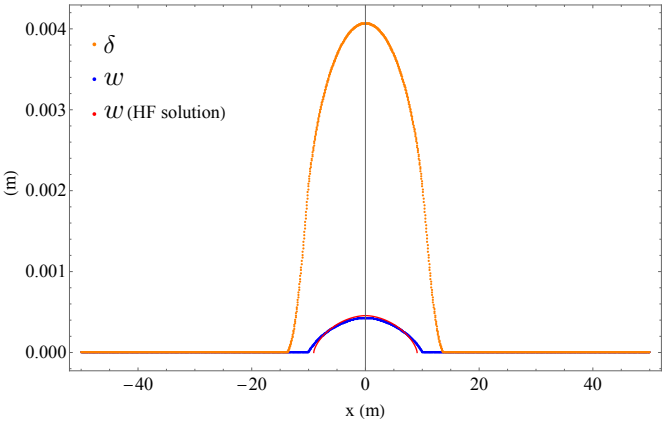

Fig. 8: Slip and fracture width profiles at $t = 1188s$ - $\mathcal{S} = 0.4$ case (Parameters set # 2 of Table 1).

jection duration (compared to the zero initial shear stress case). The relative difference of the numerical opening tip compared to this solution (not shown here for lack of space) is still above 10% at the end of this simulation.

The slip δ and opening w profiles along the pre-existing fracture (at the final time step of the simulation) displayed in Fig. 8 confirm that the shear slip continues to accumulate in the opening zone as the initial shear stress is completely released in that part of the fracture (which grows in time).

5 CONCLUSIONS

We have investigated under a plane-strain configuration the transition from a strictly frictional rupture to a hydraulic fracture for the case of a fluid injection at a constant rate. This scenario is relevant for practical hydraulic stimulation of a pre-existing fracture as the shear rupture is often accompanied by fracture opening.

We have notably shown (analytically and numerically) that at times greater than a characteristic time t_p (Eq. 25), the position of the frictional rupture tip ℓ_s ultimately tracks the growth of the hydraulic fracture front ℓ: $\ell_s = \lambda(\mathcal{S})\ell$, $\lambda \geq 1$ (see Fig 2). The numerical results presented here needs to be investigated further, notably to establish the convergence toward the late-time limit better. In addition, the numerical results shown in this work highlights the impact of the "leaky" tip condition at the opening front - which is ultimately related to the initial interface permeability. Additional numerical and scaling analysis are required to fully understand its implication on the growth of the opening front, notably when the initial fracture permeability is larger.

We would like to also highlight that our numerical solver has been verified here against analytical solutions in different limiting regimes (solely frictional and solely opening mode fluid-driven ruptures). From our experience, this work reinforces the importance of in-depth comparison with existing solutions (valid for limiting regimes) for multi-physics fracture propagation problems in order

to verify numerical solvers properly.

In future contributions, the impact of shear-induced dilatancy (and the associated permeability changes) needs to be investigated in more detail, notably with respect to its impacts: (a) on opening and shear crack tips propagation and (b) the ultimate increase of hydraulic transmissibility of the pre-existing fracture.

Acknowledgements

The results presented here were obtained within the EMOD project (Engineering model for hydraulic stimulation). The EMOD project benefits from a grant (research contract SI/502081-01) and an exploration subsidy (contract number MF-021-GEO-ERK) of the Swiss federal office of energy for the EGS geothermal project in Haute-Sorne, canton of Jura, which is gratefully acknowledged. A.S. was partially funded by the Federal Commission for Scholarships for Foreign Students via the Swiss Government Excellence Scholarship.

REFERENCES

1. Adachi, J. I. and Detournay, E. (2002). Self-similar solution of a plane-strain fracture driven by a power-law fluid. *International Journal for Numerical and Analytical Methods in Geomechanics*, 26(6):579–604.

2. Azad, M., Garagash, D., and Satish, M. (2017). Nucleation of dynamic slip on a hydraulically fractured fault. *Journal of Geophysical Research: Solid Earth*, 122(4):2812–2830.

3. B.A. Bilby and J.D. Eshelby (1968). Dislocations and the theory of fracture. In *Fracture, an Advanced Treatise*, volume I. Academic Press, New York NY.

4. Bhattacharya, P. and Viesca, R. C. (2019). Fluid-induced aseismic fault slip outpaces pore-fluid migration. *Science*, 364(6439):464–468.

5. Carslaw, H. and Jaeger, J. (1959). *Conduction of heat in solids*. Oxford Univ Press.

6. Ciardo, F. and Lecampion, B. (2019). Effect of dilatancy on the transition from aseismic to seismic slip due to fluid injection in a fault. *Journal of Geophysical Research: Solid Earth*, 124:3724—3743.

7. Ciardo, F. and Lecampion, B. (2023). Injection-induced aseismic slip in tight fractured rocks. *Rock Mechanics and Rock Engineering*, pages 1–22.

8. Ciardo, F., Lecampion, B., Fayard, F., and Chaillat, S. (2020). A fast boundary element based solver for localized inelastic deformations. *Int. J. Numer. Meth. Engng*.

9. Detournay, E. (2004). Propagation regimes of fluid-driven fractures in impermeable rocks. *International Journal of Geomechanics*, 4(1):35–45.

10. Detournay, E. (2016). Mechanics of hydraulic fractures. *Annual Review of Fluid Mechanics*, 48:311–339.

11. Garagash, D. I. and Detournay, E. (2005). Plane-strain propagation of a fluid-driven fracture: small toughness solution. *ASME Journal of Applied Mechanics*, 72:916–928.

12. Garagash, D. I. and Germanovich, L. N. (2012). Nucleation and arrest of dynamic slip on a pressurized fault. *Journal of Geophysical Research: Solid Earth (1978–2012)*, 117(B10).

13. Guglielmi, Y., Nussbaum, C., Jeanne, P., Rutqvist, J., Cappa, F., and Birkholzer, J. (2020). Complexity of fault rupture and fluid leakage in shale: Insights from a controlled fault activation experiment. *Journal of Geophysical Research: Solid Earth*.

14. Hackbusch, W. (2015). *Hierarchical matrices: algorithms and analysis*, volume 49. Springer.

15. Hayashi, K. and Abe, H. (1982). Opening of a fault and resulting slip due to injection of fluid for the extraction of geothermal heat. *Journal of Geophysical Research: Solid Earth*, 87(B2):1049–1054.

16. Hills, D. A., Kelly, P. A., Dai, D. N., and Korsunsky, A. M. (1996). *Solution of crack problems: the distributed dislocation technique*, volume 44 of *Solid Mechanics and its Applications*. Kluwer Academic Publ., Dordrecht.

17. Jung, R. (2013). EGS - Goodbye or Back to the Future. In *ISRM International Conference for Effective and Sustainable Hydraulic Fracturing*. International Society for Rock Mechanics.

18. McClure, M. W. and Horne, R. N. (2014). An investigation of stimulation mechanisms in Enhanced Geothermal Systems. *Int. J. Rock Mech. Min. Sci.*, 72:242–260.

19. Mogilevskaya, S. G. (2014). Lost in translation: Crack problems in different languages. *International Journal of Solids and Structures*, 51(25):4492–4503.

20. Mroz, Z. and Giambanco, G. (1996). An interface model for analysis of deformation behaviour of discontinuities. *International Journal for Numerical and Analytical Methods in Geomechanics*, 20(1):1–33.

21. Plesha, M. (1995). Rock joints: Theory, constitutive equations. *Studies in Applied Mechanics*, 42(C):375–393.

22. Rice, J. and Cleary, M. (1976). Some basic stress diffusion solutions for fluid-saturated elastic porous media with compressible constituents. *Rev. Geoph.*, 14(2):227–241.

23. Rice, J. R. (1968). Mathematical analysis in the mechanics of fracture. In H. Liebowitz, editor, *Fracture: An Advanced Treatise*, volume 2, chapter 3, pages 191–311.

24. Sáez, A., Lecampion, B., Bhattacharya, P., and Viesca, R. (2022). Three-dimensional fluid-driven stable frictional ruptures. *J. Mech. Phys. Sol.*, 160:104754.

25. Sheng, D. and Sloan, S. (2003). Time stepping schemes for coupled displacement and pore pressurē analysis. *Computational Mechanics*, 31(1):122–134.

26. Stupkiewicz, S. and Mróz, Z. (2001). Modeling of friction and dilatancy effects at brittle interfaces for monotonic and cyclic loading. *Journal of Theoretical and Applied Mechanics*, 39:707–739.

27. Viesca, R. C. (2021). Self-similar fault slip in response to fluid injection. *Journal of Fluid Mechanics*, 928:A29.

28. Witherspoon, P. A. and Wang, J. S.Y. and Iwai, K. and Gale, J. E. (1980). Validity of cubic law for fluid flow in a deformable rock fracture. *Water Resources Res.*, 16(6):1016–1024.